BESIII Analysis Memo

DocDB-497

BAM-228

July 17, 2019

Amplitude analysis of $D_s^+ \to K^+ K^- \pi^+$

Meng Wang[a], Yu Lu[a], and Liaoyuan Dong[a], and Huaimin Liu[a]

[a]*Institute of High Energy Physics, CAS*

Internal Referee Committee

Ref1 xx (Chair)[d], Ref2 xx[e], and Ref3 xx[f]

[d]*Department of Computer Science and Engineering*
[e]*Department of Electrical Engineering*
[f]*Latex Univeristy*

Abstract

We have performed an amplitude analysis of $D_s^+ \to K^+ K^- \pi^+$ using a data sample of $3.19 fb^{-1}$ recorded with BESIII detector at a center-of-mass energy of 4.178GeV. About 4000 events are used in amplitude analysis. There are 6 intermediate resonances in the model which does the best fit to data. And we also measured the branching fraction of $D_s^+ \to K^+ K^- \pi^+$ and the result is $\mathcal{B}(D_s^+ \to K^+ K^- \pi^+) = (5.47 \pm 0.07_{stat.} \pm 0.11_{sys.})\%$.

Contents

1 Introduction

1.1 The scalar meson $f_0(980)$ and $a_0(980)$

The Constituent Quark Model ahs been very successful in the past few decades by explaining how hadrons are made up. Base on this model, the nonets of pseudo-scalar, vector and tensor mesons are now well identified. However, the idenfitication of the scalar mesons is still uncertain due to the broad widths and the lack of a distincitive angular distribution. Among the candicates for the spin-parity $J^{PC} = 0^{++}$ nonet, the parameters of some states such as $f_0(980)$ and $a_0(980)$ are not well measured. For $f_0(980)$, as it is very close to $K\bar{K}$ threshold and has strong coupling to $\pi\pi$ and $K\bar{K}$ final states, its parameters are still uncertain.

According to the amplitude analysis of $D_s^+ \to \pi^+\pi^0\eta$ [1], they observed the decay $D_s^+ \to a_0(980)^0\pi^+$ and the contribution from $a_0(980)^0$ should also effect the K^+K^- $\mathcal{S}$ wave shape in the $D_s^+ \to K^+K^-\pi^+$ decay. So in this analysis, we have to take in account not only $f_0(980)$ but also $a_0(980)$ in the K^+K^- $\mathcal{S}$ wave. However, $f_0(980)$ and $a_0(980)$ are very close to each other and it is very difficutl to distinguith them without any extra input.

From the Dalitz plot analysis of $D_s^+ \to \pi^+\pi^-\pi^+$, we can get the branching fraction of D_s^+ decays to $f_0(980)\pi^+$ and then $f_0(980)$ decays to $\pi^+\pi^-$ is $\mathcal{B}(D_s^+ \to f_0(980)\pi^+, f_0(980) \to \pi^+\pi^-)$. Then if we know the the branching ratio of $\Gamma_{f_0(980)}(K^+K^-)/\Gamma_{f_0(980)}(\pi^+\pi^-)$, it is easy to obtain:

$$\mathcal{B}(D_s^+ \to f_0(980)\pi^+, f_0(980) \to K^+K^-) = \mathcal{B}(D_s^+ \to f_0(980)\pi^+, f_0(980) \to \pi^+\pi^-)\frac{\Gamma_{f_0(980)}(K^+K^-)}{\Gamma_{f_0(980)}(\pi^+\pi^-)}. \quad (1)$$

In a similar way, we can obtain:

$$\mathcal{B}(D_s^+ \to a_0(980)\pi^+, a_0(980) \to K^+K^-) = \mathcal{B}(D_s^+ \to a_0(980)\pi^+, a_0(980) \to \pi^0\eta)\frac{\Gamma_{a_0(980)}(K^+K^-)}{\Gamma_{a_0(980)}(\pi^0\eta)}. \quad (2)$$

Then, obviously, the ratio of fit fractions of $D_s^+ \to f_0(980)\pi^+$ and $D_s^+ \to a_0(980)\pi^+$ Γ is:

$$\Gamma = \frac{\mathcal{B}(D_s^+ \to f_0(980)\pi^+, f_0(980) \to \pi^+\pi^-)\frac{\Gamma_{f_0(980)}(K^+K^-)}{\Gamma_{f_0(980)}(\pi^+\pi^-)}}{\mathcal{B}(D_s^+ \to a_0(980)\pi^+, a_0(980) \to \pi^0\eta)\frac{\Gamma_{a_0(980)}(K^+K^-)}{\Gamma_{a_0(980)}(\pi^0\eta)}}. \quad (3)$$

If we can get the value of Γ in Eq. 3, it's possible to fix the ratio in amplitude analysis and then distinguith $f_0(980)$ and $a_0(980)$ at the low end of K^+K^- mass spectrum. Using isopin relations, the relation between $\Gamma_{f_0(980)}(\pi\pi)/\Gamma_{f_0(980)}(\pi\pi + K\bar{K})$ and $\Gamma_{f_0(980)}(K^+K^-)/\Gamma_{f_0(980)}(\pi^+\pi^-)$ is:

$$\frac{\Gamma_{f_0(980)}(K^+K^-)}{\Gamma_{f_0(980)}(\pi^+\pi^-)} = \frac{3}{4} \cdot \left[\frac{1}{\frac{\Gamma_{f_0(980)}(\pi\pi)}{\Gamma_{f_0(980)}(\pi\pi)+\Gamma_{f_0(980)}(K\bar{K})}} - 1 \right]. \quad (4)$$

However the value of $\Gamma_{f_0(980)}(K^+K^-)/\Gamma_{f_0(980)}(\pi^+\pi^-)$ is not well measured as is shown in following Table 1 from Ref. [12]. So we have to extract the $\mathcal{S}$ wave line shape at the low end of K^+K^- mass spectrum in a quasi-model-independent way. In other words, we take $a_0(980)$ and $f_0(980)$ as a whole.

Table 1: The $f_0(980)$ branching ratio $\Gamma_{f_0(980)}(\pi\pi)/\left[\Gamma_{f_0(980)}(\pi\pi) + \Gamma_{f_0(980)}(K\bar{K})\right]$

VALUE	TECN	COMMENT
0.52 ± 0.12	BABR	$B^{\pm} \to K^{\pm}\pi^{\pm}\pi^{\mp}$ [2]
$0.75^{+0.11}_{-0.13}$	BES2	$\chi_{c0} \to 2\pi^{+}2\pi^{-}, \pi^{+}\pi^{-}K^{+}K^{-}$ [3]
0.84 ± 0.02	SPEC	Combined fit [4]

1.2 The $D_s^+ \to K^+K^-\pi^+$ decay

The decay $D_s^+ \to K^+K^-\pi^+$ is a Cabibbo-favored (CF) channel and has a large branching fraction for the D_s meson. Thus, this decay channel is usually used to normalize measurements of decay chains involving charm quarks. Fig. 1 illustrates main Feynman diagrams related to the decay. The main contri-
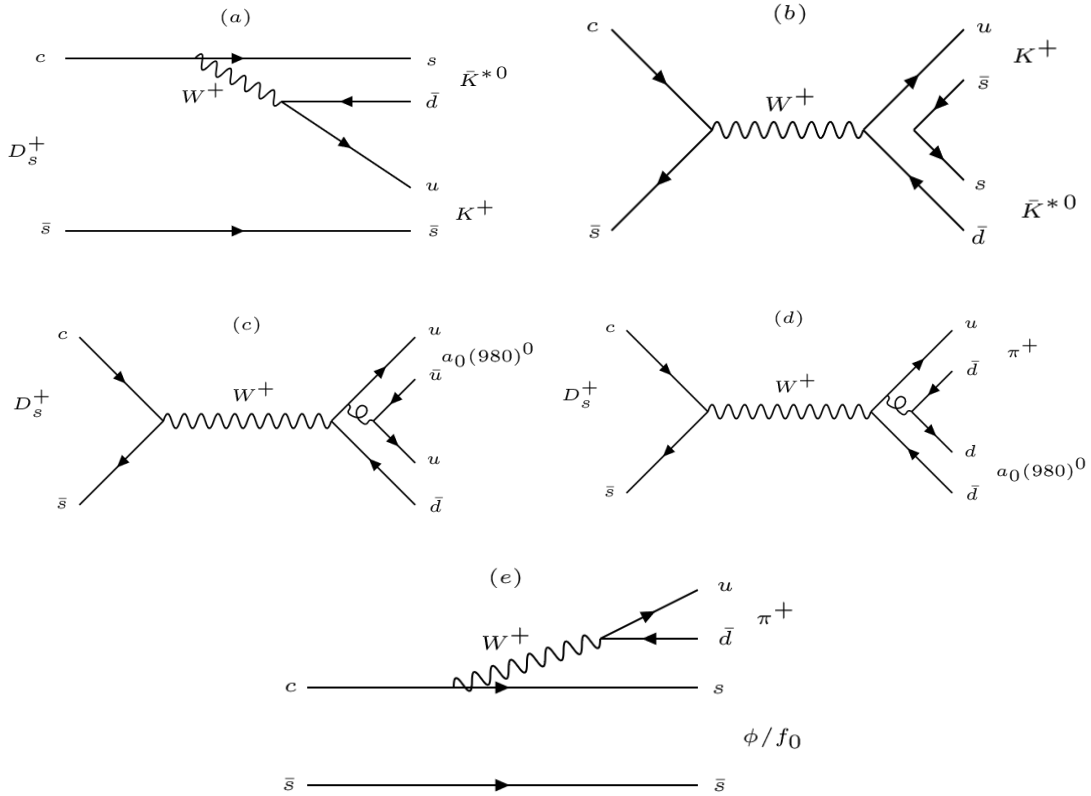
Figure 1: Main Feynman diagrams associated with $D_s^+ \to K^+K^-\pi^+$ decay.

bution comes from the diagram with an internal W^+ emission(Fig. 1(a) and Fig. 1(b)), that describes the $D_s^+ \to \bar{K}^*(892)^0K^+$ decay, and the diagram with an external W^+ emission(Fig. 1(e)), that describes the diagram $D_s^+ \to \phi\pi^+/f_0\pi^+$, and the diagram with W-annihilation(Fig. 1(c) and Fig. 1(d)), that describes the decay $D_s \to a_0(980)^0\pi^+$.

Table 2: previous analyses of this decay channel.

Decay mode	Fit fraction(BABAR)	Fit fraction(CLEO-c)	Fit fraction(E687)
$D_s^+ \to \bar{K}^*(892)^0 K^+$	47.9±0.5±0.5	47.4±1.5±0.4	47.8±4.6±4.0
$D_s^+ \to \phi(1020)\pi^+$	41.4±0.8±0.5	42.2±1.6±0.3	39.6±3.3±4.7
$D_s^+ \to f_0(980)\pi^+/a_0(980)\pi^+$	16.4±0.7±2.0	28.2±1.9±1.8	11.0±3.5±2.6
$D_s^+ \to \bar{K}_0^*(1430)^0 K^+$	2.4±0.3±1.0	3.9±0.5±0.5	9.3±3.2±3.2
$D_s^+ \to f_0(1710)\pi^+$	1.1±0.1±0.1	3.4±0.5±0.3	3.4±2.3±3.5
$D_s^+ \to f_0(1370)\pi^+$	1.1±0.1±0.2	4.3±0.6±0.5	...
$\sum FF(\%)$	110.2±0.6±2.0	129.5±4.4±2.0	111.1
χ^2/NDF	$\frac{2843}{2305-14} = 1.2$	$\frac{178}{117} = 1.5$	$\frac{50.2}{33} = 1.5$
Events	96307 ± 369	12226 ± 22	701 ± 36

1.3 Amplitude analysis

Knowledge of the decay amplitude allows us to properly account for interference effects when measuring absolute hadronic branching fractions of D_s mesons. Amplitude analysis of this decay can help us to understand the interference effects and so an amplitude analysis is necessary. Below is the table of previous analyses of this decay channel.

From Table2 [5], we can see an obvious difference of decay fraction of $f_0(980)\pi^+$ between BARBAR and CLEO-c. E687 used about 700 events and the E687 model did not take $f_0(1370)\pi^+$ into account. For CLEO-c, about 14400 events with purity about 84.9% were selected with single tag method. The analysis of BARBAR used about 100000 events with purity about 95%. In this analysis with double tag method, we can get a nearly background free data sample, that will be good to perform the amplitude analysis.

2   Data Set and Monte Carlo Samples

We use 3.195 fb^{-1} data set collected at E_{cm} = 4.178GeV by BESIII detector in 2016. Both data sample and Monte Carlo samples are reconstructed under BOSS7.0.3. All samples were generated with run-dependent E_{cm} [7], except for the Bhabha, $\mu - pair$ and Two-photon fusion events. For these three types of events, we used a constant E_{cm} at 4178.37MeV which is twice of a luminosity-weighted average of the measured beam energy in the center-of-mass frame. Totally 40 rounds of generic MC with each round equaling to data size are used for background study, tag efficiencies estimation(rounds 01-30) and input-output check for branching fraction measurement(rounds 31-40). They are avaulable at /besfs3/offline/data/703-1/4180/mc/. For each round of generic MC, the detail component and corresponding size of each Monte Carlo sample are shown in Table 3.

Table 3: Component and corresponding size, assume luminosity = 3195/pb.

Component	cross section (pb)	Size(M)	directory
D^0D^0	179	0.5719	D0D0
D^+D^-	197	0.6294	DpDm
$D^{*0}D^0$	1211	3.8691	DST0D0
$D^{*+}D^-$	1296	4.1407	DSTpDm
$D^{*0}D^{*0}$	2173	6.9427	DST0DST0
$D^{*+}D^{*-}$	2145	6.8533	DSTpDSTm
$D_s^+D_s^-$	7	0.0225	DsDs
$D_s^{*+}D_s^-$	961	3.0700	DsSTDs
$DD^*\pi^+$	383	1.2237	DDSTPIp
$DD^*\pi^0$	192	0.6134	DDSTPI0
$DD\pi^+$	50	0.1598	DDPIp
$DD\pi^0$	25	0.0799	DDPI0
Component	cross section (nb)	Size(M)	
$q\bar{q}$	13.8	44.0910	qq
$\gamma J/\psi$	0.40	1.2780	RR1S
$\gamma\psi(2S)$	0.42	1.3419	RR2S
$\gamma\psi(3770)$	0.06	0.1917	RR3770
$\tau\tau$	3.45	11.0228	tt
$\mu\mu$	5.24	16.7418	mm
ee	423.99	13.5465(0.01×)	ee
$\gamma\gamma$	1.7	5.4315	TwoGam
HCT	0.10178	0.3252	HCT

For the Signal MC, we generate the signal events with one D_s decaying to signal mode using the generator "DIY", in which the parameters are obtained from the fit to data. PHSP MC and Signal MC are used in MC integration required for the amplitude fit. The Signal MC is also used in the input/output check.

3 Event Selection

At $E_{cm} = 4.178 GeV$, pairs of $D_s D_s^*$ are produced, and the D_s^* decays to either $D_s \gamma$ or $D_s \pi^0$. We use double tag method to select our signal events.

3.1 Tracking, PID, $\pi^0/\eta^{(')}$ and K_S^0 Rconstruction

D_s candicates are built from $K^\pm$, $\pi^\pm$, $\pi^0/\eta^{(')}$ and K_S^0. The selections of the particles to build D_S candicates are performed with DTagAlg-00-01-05 package with the default setting, which are summarized below.

- Tracking:

  - The properties of charged tracks are determined based on the MDC information. Charged track candidates must satisfy:

    - $|cos\theta| < 0.93$.

    - $|dr| < 1cm$ and $|dz| < 10cm$,

      where $|dr|$ and $|dz|$ are defined as the one reconstructed minus the interaction point.

- Particle ID:

  - Charged tracks are identified as pion or kaon with Particle Identification (PID), which is implemented by combing the information of the energy loss (dE/dx) in MDC and the time-of-flight measured from the TOF system. Kaon and Pion are identified with the requirements that

    - *Prob(K) > 0* and *Prob(K) > Prob(π)* for *K*,

    - *Prob(π) > 0* and *Prob(π) > Prob(K)* for *π*, where *Prob(X)* is the probability of hypothesis X, X can be π or *K*.

- π^0/η selection: π^0 candidates are reconstructed through $\pi^0 \rightarrow \gamma\gamma$ with package of PioEtaToGGRecAlg. The photons are reconstructed as energy showers on the EMC. We require:

  - Minimum energy for barrel showers($|cos\theta| < 0.8$): $E_{min} > 25 MeV/c^2$,

  - Minimum energy for endcap showers($0.86 < |cos\theta| < 0.92$): $E_{min} > 50 MeV/c^2$,

  - Shower within other $|cos\theta|$ regions are rejected.

  - EMC time requirements for events with at least one charged track detected: $0 \le t \ge 14$(50ns),

Then we perform a constrained fit on the photon pairs to the nominal π^0/η mass and require:

- The unconstrained invariant mass for π^0: $0.115 < M(\gamma\gamma) < 0.015 GeV/c^2$,

- The unconstrained invariant mass for η : $0.490 < M(\eta) < 0.580 GeV/c^2$,

- Mass fit: $\chi^2_{1c} < 30$.

- $\eta^{'}$ selection: The $\eta^{'}$ candidates are reconstructed with $\pi^+\pi^-\eta$, the invariant mass for $\pi^+\pi^-\eta$ is required to fall into the range of $[0.938, 0.978] GeV^2$.

- K^0_S selection: K^0_S candidates are reconstructed using VeeVertexAlg package with two opposite charged tracks with requiring:

    - $|cos\theta| < 0.93$

    - $|dz| < 20 cm$

For each pair of tracks, a constrained vertex fit is performed and the track parameters' results are used to get the invariant mass $M(K^0_S)$. Then the decay length of K^0_S is obtained with second vertex fit by the SecondVertexFit package. For K^0_S selection, we require:

    - $0.487 GeV/c^2 < M(K^0_S) < 0.511 GeV/c^2$.

    - Significance of the K^0_S decay lenght has two standard deviations.

- D_s selection: According to the MC study on D_s reconstruction (BESSIII-DocDB-380), the D_s candidates fall into the mass window of $1.90 < m_{D_s} < 2.03 GeV/c^2$ and the corresponding M_{rec} satisfied $2.051 < M_{rec} < 2.180 GeV/c^2$ are retained for further study. In which, the definition of M_{rec} is

$$M_{rec} = \sqrt{(E_{cm} - \sqrt{p^2_{D_s} + m^2_{D_s}})^2 - |\vec{p}_{cm} - \vec{p}_{D_s}|^2} \, , \qquad (5)$$

where E_{cm} is the energy of initial state, calculated from the beam energy [7], $\vec{p}_{D_s}$ is the momentum of D_s candidate, m_{D_s} is D_s mass quoted from PDG [8] and $\vec{p}_{cm}$ and $\vec{p}_{D_s}$ are four-momentum of initial state and the decay products of a D_s candidate, respectively.

3.2 Sigal Selection

We use different methods to select events in model indepent analysis(Sec.4.1), amplitude analysis(Set.5.1) and branching fraction measurement(Set.6.1). And the details are in the correspongding sections.

4 Model Independent Partial Wave Analysis

In the K^+K^- threshold both $a_0(980)$ and $f_0(980)$ can be present, and both resonances have very similar parameters which suffer from large uncertainties. In this section we obtain model-independent information on the K^+K^-S wave by performing a MIPPPWA(model indendent partial wave analysis) in the K^+K^- threshold region.

4.1 Signal Candidate Selection

After the selection in Set.3, we continue to select signals for model independent partial wave analysis. As MIPWA need more data events, we do not requre D_s^+ and D_s^- appear in pairs. Before selecting the best candidate, we vote the candidates with $\pi^\pm(\pi^0)$ whose momentum is less than $0.1GeV$ to remove soft $\pi^\pm(\pi^0)$ from D^* decays. For every candidates of D_s decays, all tracks at signal side are added to apply kinematric fitting. Only mass of D_s from signal side is constrained.Then we select the candidate with minimum χ^2_{1c}.

4.2 Background Analysis

In order to further suppress the background, the multiple-variable analysis (MVA) is used. We train MVA methos separately with different sets of variables for the two event categories depending on the D_s^+ origin. Sideband region used below is defined as the region of $1.90 < M(D_s) < 1.952GeV$ and $1.985 < M(D_s) < 2.03GeV$, $M(D_s)$ is the invariant mass of D_s. And the signal region is $1.952 < M(D_s) < 1.985GeV$. These two categories of events are selected in a $M_{rec} - \Delta M$ 2D plane shown in Fig.2:

- Cat. #0: Direct D_s^+. We use the following variables whose distributions for signal and background are shown in Fig.3,

  1. M_{rec},

  2. P_{rest}, defined as the total momentum of the tracks and neutrals in the rest of event (not part of the $D_s^+ \rightarrow K^+K^-\pi^+$ candidate),

  3. E_γ, defined as the energy of gamma from D_s^*.

  From Fig. 3(generic MC) and Fig.4(data), we can see that the corresponding distributions of these variables of data and generic MC are roughly consistent.

- Cat. #1: Indirect D_s^+. We use the following variables whose distributions for signal and background are shown in Fig.5,
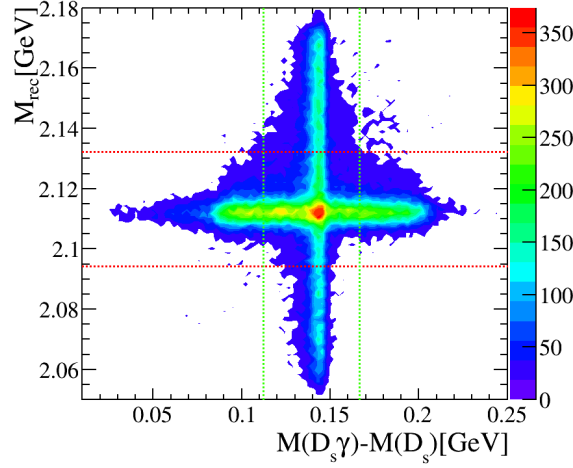
Figure 2: Two dimensional plane of M_{rec} versus $\Delta M \equiv M(D_s^+\gamma) - M(D_s^+)$ from the simulated $D_s^+ \to K^+K^-\pi^+$ decyas. The red(green) dashed lines mark the mass window for the D_s^+ Cat. #0(Cat. #1) around the $M_{rec}(\Delta M)$ peak.

1. ΔM,

2. M'_{rec}, defined as $M'_{rec} = \sqrt{\left(E_{cm} - \sqrt{p_{D_s\gamma}^2 + m_{D_s^*}^2}\right)^2 - p_{D_s\gamma}^2}$, with $p_{D_s\gamma}$ as the momentum of the $D_s\gamma$ combination, $m_{D_s^*}$ as the nominal D_s^* mass,

3. N_{tracks}, defined as the total number of tracks and neutrals in an event.

From Fig. 5(generic MC) and Fig.6(data), we can see that the corresponding distributions of these variables of data and generic MC are roughly consistent.
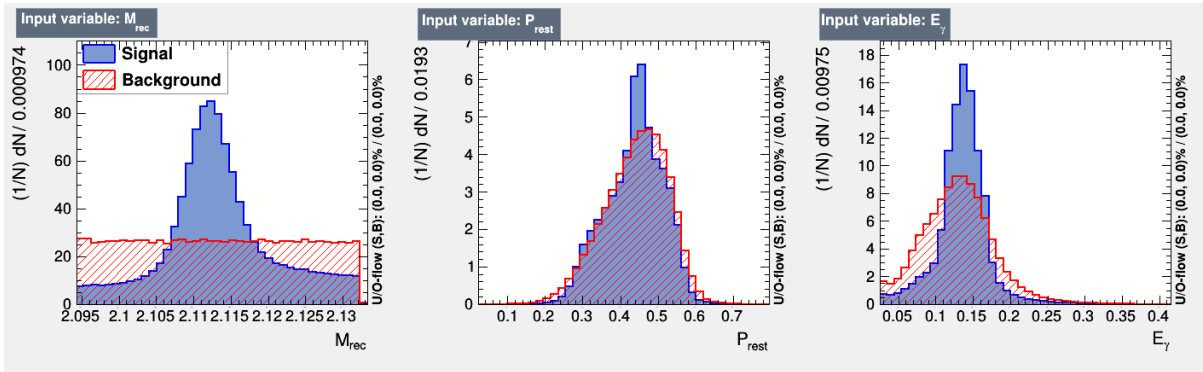

Figure 3: For event Cat. #0, distributions of MVA variables from simulated signal decays and background events.

As the results shown in Fig.7, this BDTG training and test samples are well matched. For event Cat. #0 (Cat. #1), the sample with BDTG value larger than 0.33(0.65) is retained for further study.
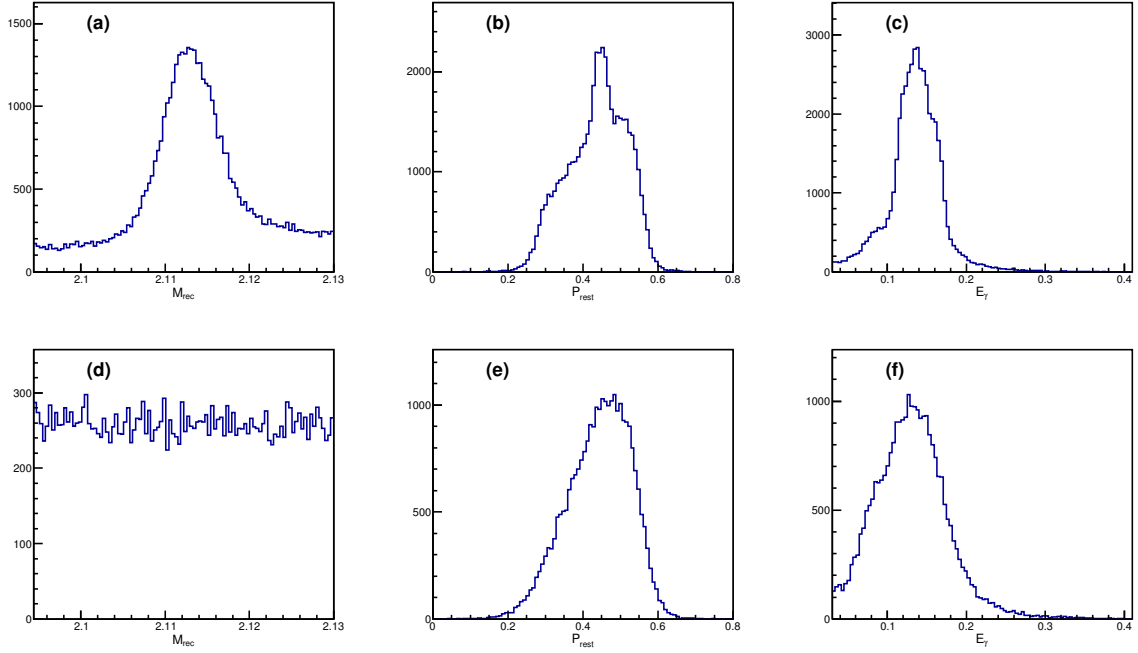
Figure 4: The distribution(Cat. #0) of these three observables ((a) and (d)) M_{rec}, ((b) and (e)) P_{rest} and ((c) and (f)) E_γ for((a), (b) and (c)) Signal and ((d), (e) and (f)) Sideband regions from data are shown.

After applying the BDTG requirement, the background shows no obviously peak around the region of [1.95, 1.982] GeV (Signal region), which are shown in Fig.8. The fit to the signal D_s invariant mass ($M_{D_s^2}$) spectrum gives the background yield in Signal region is 73.6 ± 18.7, shown as in Fig.9. In the fit, the signal shape is the MC shape convoluted with a Gaussian function and the background is described with 1st-order Chebychev polynomial.

The projections of the "Sideband"($1.90 < M(D_s) < 1.95 GeV$ and $1.985 < M(D_s) < 2.03 GeV$) from data and generic MC after signal events removed are shown in Fig.10. The corresponding plots agree well.

Thus the generic MC sample with signal events removed is used to subtract the background in MIPWA.

4.3 MIPWA method

Let N be the number of events for a given mass interval $I = [m_{K^+K^-}; m_{K^+K^-} + dm_{K^+K^-}]$. We write the corresponding angular distributions in terms of the appropriate spherical harmonic functions as

$$\frac{dN}{d\cos\theta} = 2\pi \sum_{k=0}^{L} \left\langle Y_k^0 \right\rangle Y_k^0(\cos\theta), \tag{6}$$
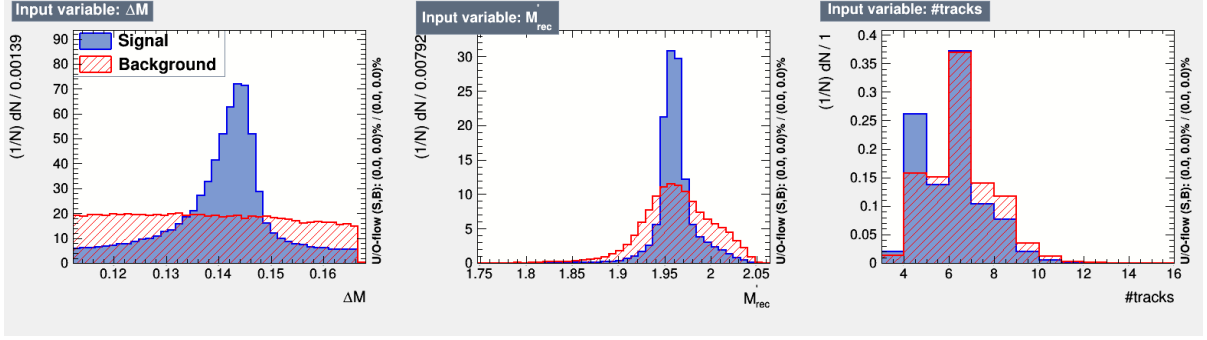
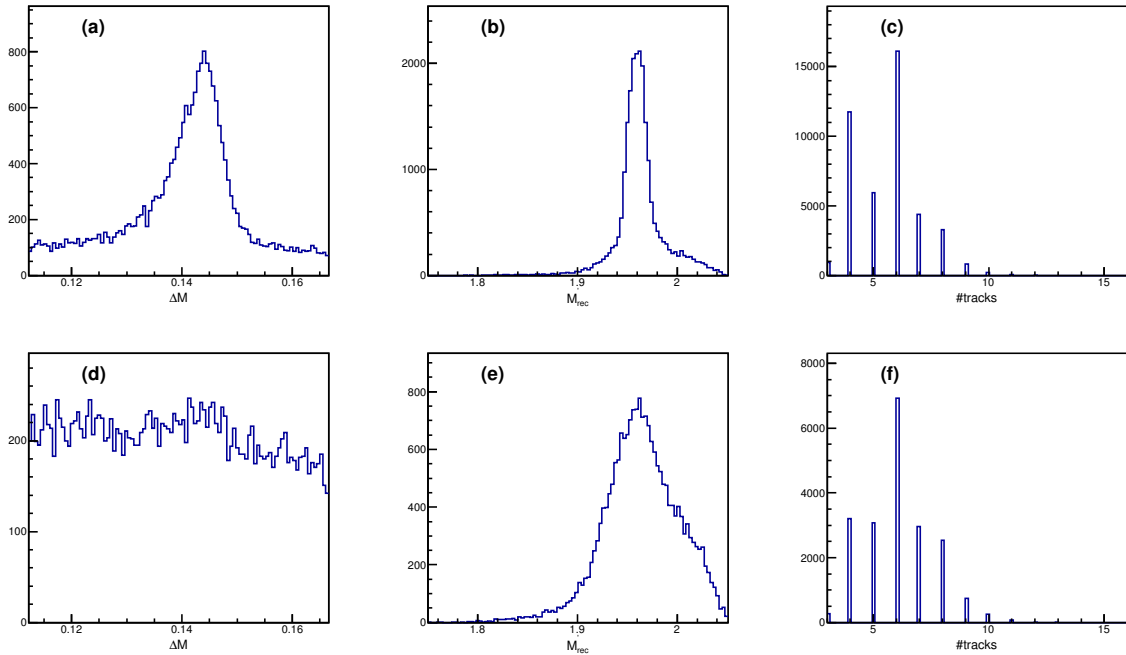Figure 5: For event Cat. #1, distributions of MVA variables from simulated signal decays and background events.

Figure 6: The distribution(Cat. #1) of these three observables ((a) and (d)) M_{rec}, ((b) and (e)) P_{rest} and ((c) and (f)) E_γ for((a), (b) and (c)) Signal and ((d), (e) and (f)) Sideband regions from data are shown.

where $L - 2\ell_{max}$, and ℓ_{max} is the maximum orbital angular momentum quantum number required to describe the K^+K^- system at $m_{K^+K^-}$ (e.g. $\ell_{max} =1$ for S-, P-wave description); θ is the angle between the K^+ direction in the K^+K^- system in the D_s^+ rest frame. The normalizations are such that

$$\int_{-1}^{1} Y_k^0(\cos\theta)Y_j^0(\cos\theta), d\cos\theta = \frac{\delta_{kj}}{2\pi}, \quad (7)$$

and it is assumed that the distribution $\frac{dN}{d\cos\theta}$ has been efficiency corrected and background subtracted. Using this orthogonality condition, the coefficiencies in the expansion are obtained from

$$\langle Y_k^0 \rangle = \int_{-1}^{1} \frac{dN}{d\cos\theta} d\cos\theta, \quad (8)$$
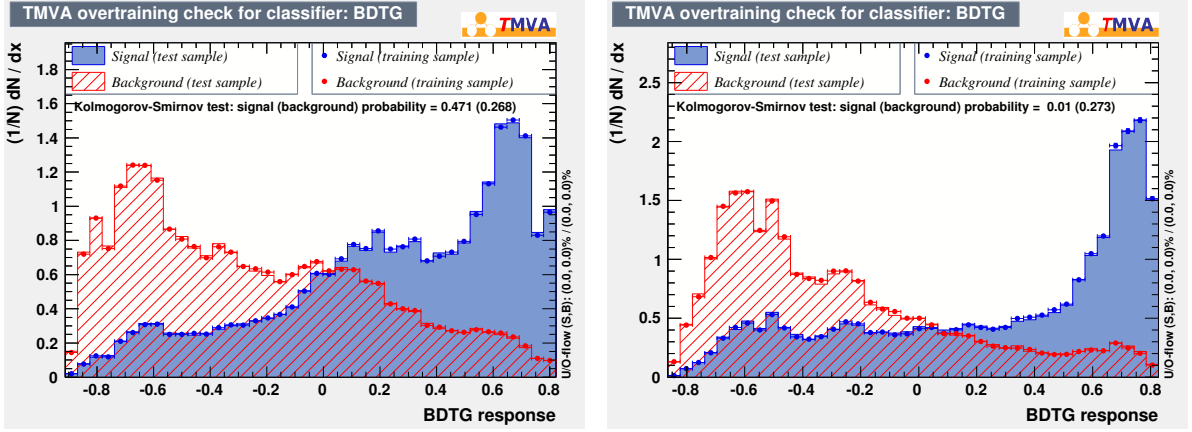
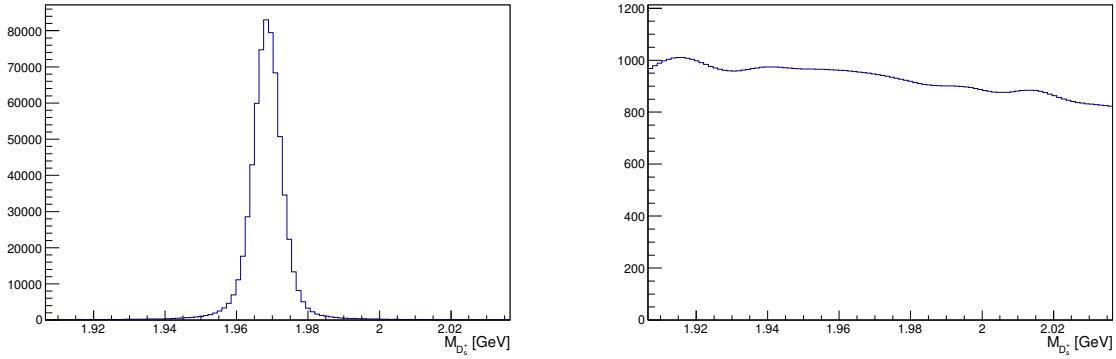Figure 7: The comparisions between the training and test samples.

Figure 8: The signal and background distributions from generic MC after BDTG requirement.

where the intergral is given, to a good approximiation, by $\sum_{n=1}^{N} Y_k^0(\cos\theta_n)$, where θ_n is the value of θ for the n-th event.

Fig.11 shows the K^+K^- mass spectrum up to 1.15 GeV weighted by $Y_k^0(\cos\theta) = \sqrt{(2k+1)/(4\pi)}P_k(\cos\theta)$ for k=0, 1, and 2, where P_k is the Legendre ploynomial function of orkder k. These distributions are corrected for efficiency and phase space, and background is subtracted using background from generic MC after BDTG requirement.

The number of events N for the mass interval I can be expressed also in terms of the partial-wave amplitudes describing the K^+K^- system. Assuming that only S- and P-wave amplitudes are necessary in this limited region, we can write:

$$\frac{dN}{d\cos\theta} = 2\pi \left| S\,Y_0^0(\cos\theta) + P Y_1^0(\cos\theta) \right|^2 . \tag{9}$$

By comparing Eqa. 6 and 9, we obtain

$$\begin{aligned} \sqrt{4\pi}\left\langle Y_0^0 \right\rangle &= |S|^2 + |P|^2 , \\ \sqrt{4\pi}\left\langle Y_2^0 \right\rangle &= \frac{2}{\sqrt{5}}|P|^2 , \end{aligned} \tag{10}$$
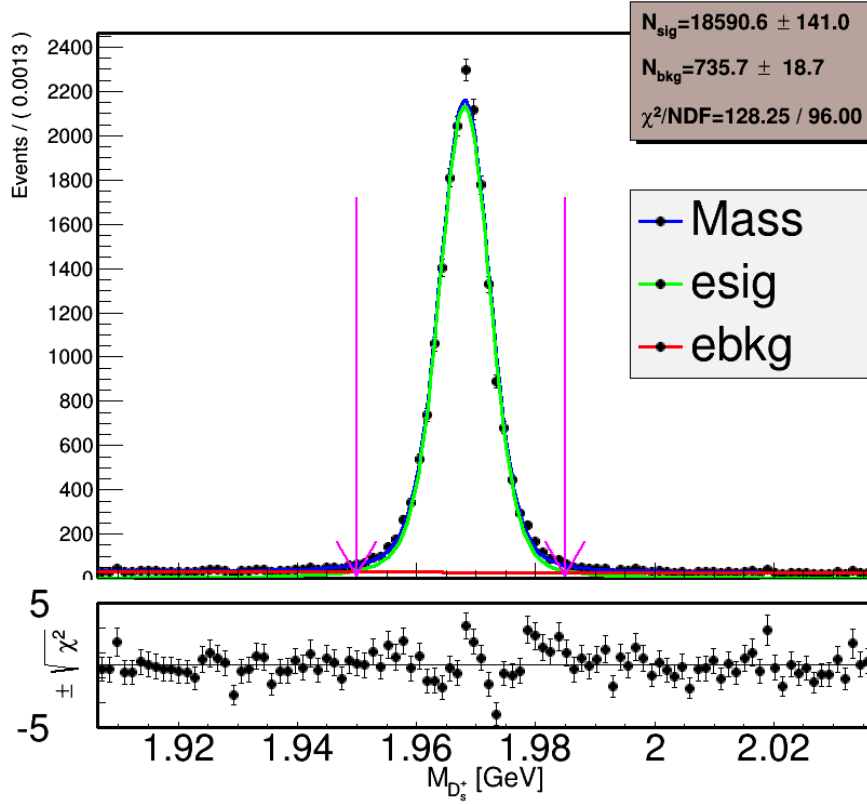
Figure 9: The fit to the signal D_s invariant mass (M_{D_s}) spectrum after BDTG requirement, the area between the pink arrows is the signal area of the sample for MIPWA.

1 The above system of equations can be solved in each interval of K^+K^- invariant mass for $|S|$ and $|P|$

2 and the resulting distributions are shown in Fig.12.

4.4 S-wave parameterization at the K^+K^- threshold

4 We empirically parameterize the $f_0(980)$ with the following function:

$$A_{f_0(980)/a_0(980)} = \frac{1}{m_0^2 - m^2 - im_0\Gamma_0\rho_{KK}}, \tag{11}$$

5 where $\rho_{KK} = 2p/m$, and obtain the flollowing parameter values:

$$m_0 = (0.919 \pm 0.006_{stat})GeV,$$
$$\Gamma_0 = (0.272 \pm 0.040_{stat})GeV. \tag{12}$$

6 The errors are statistical only. The fit result are shown in Fig.13.
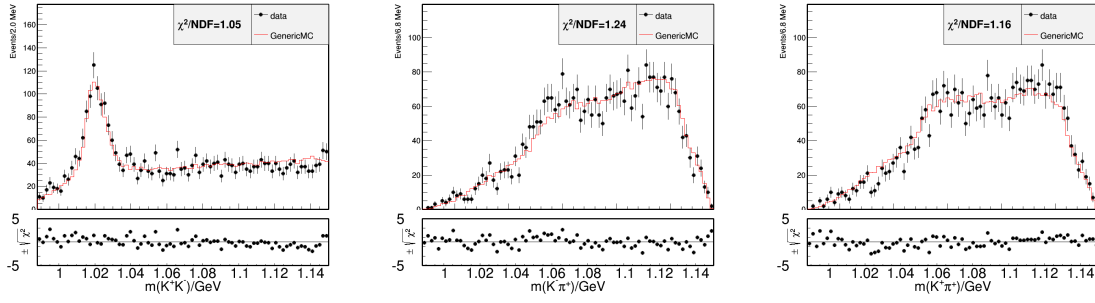
Figure 10: The projections of $m(K^+K^-)$, $m(K^-\pi^+)$, $m(K^+\pi^+)$ from "Sideband" for data(dots with error bars) and generic MC after signal events removed (red histogram) after BDTG requirement.

Figure 11: K^+K^- mass spectrum in the threshold region weighted by (a) Y_0^0, (b) Y_1^0 and (c) Y_2^0, corrected for efficiency and phase space, and background subtracted.

Figure 12: Squared (a) S- and (b) P-wave amplitudes

Figure 13: Fit of squared S-wave amplitudes. the curves result from the fit described in the text.

5 Amplitude Analysis

5.1 Event Selection for Amplitude Analysis

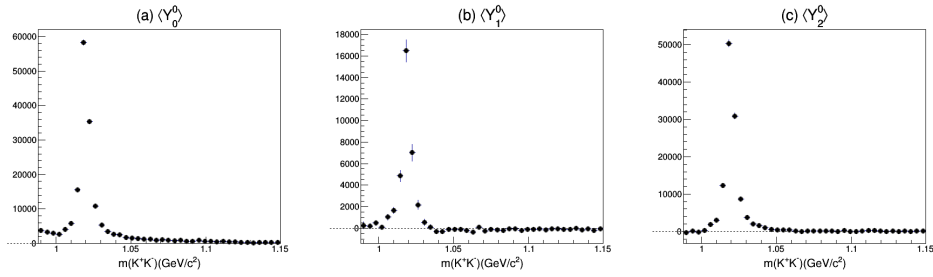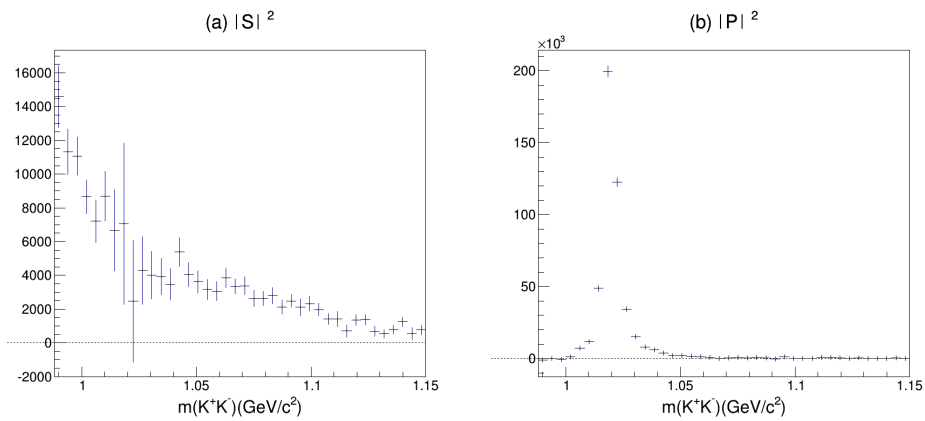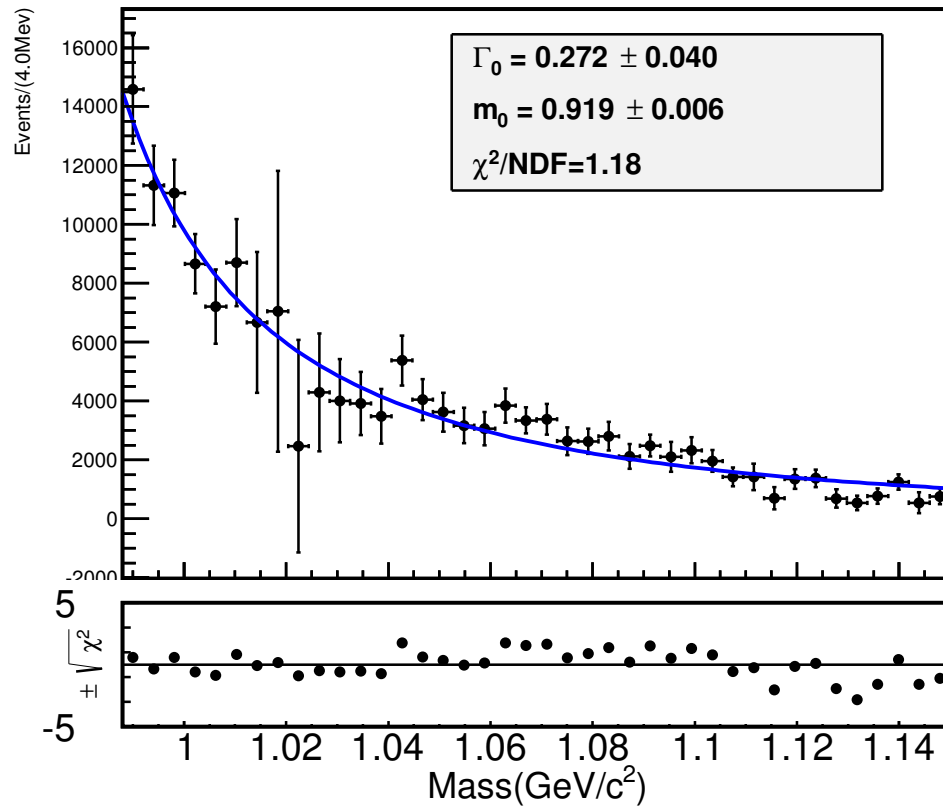After $K^{\pm}$, K^0_S, $\pi^{\pm}$ and γ are identified in Sec.3, hadronic D_s decays can be reconstructed with the DTag package. 8 tag modes are used:

$D^-_s \to K^+K^-\pi^-$, $D^-_s \to K^0_S K^-$, $D^-_s \to K^0_S K^-\pi^+\pi^-$, $D^-_s \to K^-\pi^+\pi^-$, $D^-_s \to K^0_S K^+\pi^-\pi^-$, $D^-_s \to \pi^+\pi^-\pi^-$, $D^-_s \to \eta'_{\pi^+\pi^-\eta_{\gamma\gamma}}$, $D^-_s \to K^+K^-\pi^-\pi^0$.

With the tagged D_s meson, the signal D_s is reconstructed with the remaining good tracks and good showers. The momentum of $\pi^{\pm}(\pi^0)$ is required to be larger than $100MeV/c^2$ to suppress the background of $D^* \to D\pi$. Only the D_s candidate with invariant mass falls into $[1.87, 2.06]GeV/c^2$ are selected.

For every candidate of D_s decays, all tracks at signal side and tag side as well as gamma from D^*_s are added to apply kinematic fitting. 5 constrains are added in kinematic fitting: four-momentum of $D_s D^*_s$, mass of D^*_s. Then we select the candidate with minmimum χ^2_{5c}.

The candidates satisfy:

- m_{sig} and m_{tag} falls in the mass regions shown in Table10.

- $\chi^2_{5c} < 200$

are retained for amplitude analysis, where m_{sig} and m_{tag} refer to mass of D_s at signal side and tag side respectively.

5.2 Background Analysis

We use generic MC to estimate the background. The background and signal shape of generic MC is shown in Fig.14. According to the luminosities of the data and the generic MC, after scaling the background sample to the data size, the background yiels in Signal region is 17.2. Then the fit to the signal D_s invariant mass (m_{sig}) spectrum gives the background yield in Signal region is 18.1 ± 5.1, shown as in Fig.15. The background level in MC is then consistent with the data. In the fit, the signal shape is the MC shape convoluted with a Gaussian function and the background is the MC shape.

5.3 Fit Method

The method used in amplitude analysis is the same as the Ref. [10]. In this section, we briefly review the amplitude analysis method used int this analysis.

The relative magnitudes and phases of the partial waves and the mass and width of intermediate resonances are determined by a maximum-likelihood fit to the data selected. The formulas are constructed with covariant tensors [11].
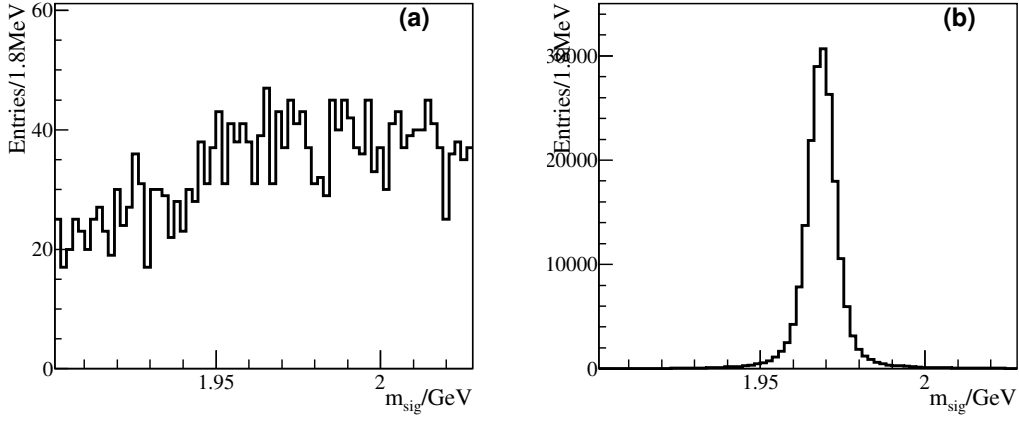
Figure 14: The background and signal shape of generic MC(round 01-40)
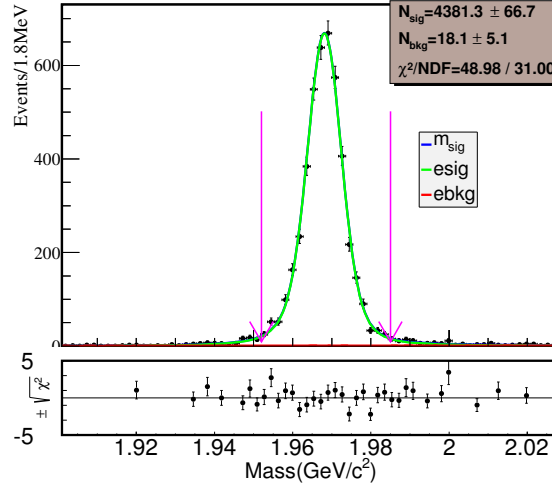
Figure 15: The fit to m_{sig} for data after selections, the area between the purple arrows is the signal area of the sample for the amplitude analysis.

Since there are three final state particles, only one possible resonant state is allowed in any intermediate process. Thus the amplitude of the nth intermediate state (A_n) is,

$$A_n = P_n S_n F_n^r F_n^D, \tag{13}$$

where S_n and $F_n^{r(D)}$ are the spin factor and the Blatt-Weisskopf barriers of the intermediate state (the D_s meson), respectively. P_n is the propagator of the intermediate resonance. For a decay process $a \rightarrow bc$, $s_{a/b/c}$ is denoted to be the invariant mass square of the particle a/b/c, and q is denoted as the magnitude of the momentum of daughter particle in the rest system of a

$$q = \sqrt{\frac{(s_a + s_b + s_c)^2}{4s_a} - s_b}. \tag{14}$$

Then for $K^*(892)^0$, $\phi(1020)^0$, $K_0^*(1430)^0$ and $f_0(1710)$, they are parameterized as a RBW,

$$
\begin{aligned}
P &= \frac{1}{(m_0^2 - s_a) - i m_0 \Gamma(m)}, \\
\Gamma(m) &= \Gamma_0 \left(\frac{q}{q_0}\right)^3 \left(\frac{m_0}{m}\right) (F^r)^2,
\end{aligned}
\tag{15}
$$

where m_0 and Γ_0 are the mass and the width of the intermediate resonances, and are fixed to the PDG values [12] except the mass and the widtch of $f_0(1370)$. The mass and width of $f_0(1370)$ are fixed to Ref. [13]. $K_0^*(1430)^0$ is parameterized with Flatte formula:

$$
P_{K_0^*(1430)^0} = \frac{1}{M^2 - s - i(g_1 \rho_{K\pi}(s) + g_2 \rho_{\eta' K}(s))},
\tag{16}
$$

where s is the $K^-\pi^+$ invariant mass squared, $\rho_{K\pi}(s)$ and $\rho_{\eta' K}(s)$ are Lorentz invariant PHSP factor, and $g_{1,2}$ are coupling constants to the corresponding final state. The parameters of $K_0^*(1430)^0$ are fixed to values measured by CLEO [14]. For resonance $f_0(980)$ & $a_0(980)$, the RBW form Eq.11 is used to describe the propagator and the values of parameters are fixed to the values in Eq.12.

The Blatt-Weisskopf barriers are given by

$$
\begin{aligned}
F_n &= 1, (S \ wave), \\
F_n &= \sqrt{\frac{z_0^2 + 1}{z^2 + 1}}, (P \ wave), \\
F_n &= \sqrt{\frac{z_0^4 + 3z_0^2 + 9}{z^4 + 3z^2 + 9}}, (D \ wave),
\end{aligned}
\tag{17}
$$

where z and z_0 are qR and q_0R, respectively. The R is the effective radius of the intermediate state or D_s meson and set to $3.0 GeV^{-1}$ for intermediate states and $5.0 GeV^{-1}$ for D_s meson [10], respectively.

As the limit of the phase space, we only consider the states with angular momenta no more than 2. As discussed in [15], the spin factor is,

$$
\begin{aligned}
S_n &= 1, (S \ wave), \\
S_n &= \tilde{T}^{(1)\mu}(D_s)\tilde{t}_\mu^{(1)}(R), (P \ wave), \\
S_n &= \tilde{T}^{(2)\mu}(D_s)\tilde{t}_\mu^{(2)}(R), (D \ wave),
\end{aligned}
\tag{18}
$$

where the $\tilde{T}^{(1)\mu}(D_s)(\tilde{T}^{(2)\mu}(D_s))$ and $\tilde{t}_\mu^{(1)}(R)(\tilde{t}_\mu^{(2)}(R))$ are the same defined in Ref. [11].

The total amplitude M is then the coherent sum of the amplitudes of intermediate processes, $M = \sum c_n A_n$, where $c_n = \rho_n e^{i\phi_n}$, is the corresponding complex coefficient. The magnitude ρ_n and phase ϕ_n are determined by the amplitude analysis. The signal PDF $f_S(p_j)$ is given by

$$
f_S(p_j) = \frac{\epsilon(p_j) \left|M(p_j)\right|^2 R_3(p_j)}{\int \epsilon(p_j) \left|M(p_j)\right|^2 R_3(p_j) \, dp_j},
\tag{19}
$$

where $\epsilon(p_j)$ is the detection efficiency parameterized in terms of the final four-momenta p_j. The index j refers to the different particles in the final states. $R_3(p_j)dp_j$ is the standard element of the three-body

phase space. The normalization intergral is determined by a MC technique,

$$\int \epsilon(p_j) \left|M(p_j)\right|^2 R_3(p_j)\, dp_j = \frac{1}{N_{MC}} \sum_{k_{MC}}^{N_{MC}} \frac{\left|M(p_j^{k_{MC}})\right|^2}{\left|M^{gen}(p_j^{k_{MC}})\right|^2}, \tag{20}$$

where k_{MC} is the index of the k_{MC}^{th} event of the MC sample and N_{MC} is the number of the selected MC events. In this analysis, a signal MC sample with about 2 million events is used in the normalization intergral calculation. $M^{gen}(p_j)$ is the PDF function used to generate the MC samples in MC integration. Firstly, the PHSP MC are used in MC integration. $M^{gen}(p_j)$ is a constant overall the phase space. Then with result obtained from the fit to data, the signal MC is then generated and used in MC integration. In the numerator of Eq.19, $\epsilon(p_j)$ is independent of the fitted variables, so it is regarded as a constant term in the fit.

Since there is only about 0.4% background in the data sample, the contribution from the background is ignored in the likelihood calculation:

$$\ln L = \sum_k^{N_{data}} \ln f_S(p_j^k), \tag{21}$$

where N_{data} is the number of candidate events in data.

5.4 Fit Fraction

The fit fractions of the individual amplitudes are calculated according to the fit results and are compared to the other measurements. In the calculation, a phase space(PHSP) MC with neither detector acceptance nor resolution involved is used. The fit fraction for an amplitude is defined as

$$FF(n) = \frac{\sum_{k=1}^{N_{gen}} |A_n|^2}{\sum_{k=1}^{N_{gen}} \left|M(p_j^k)\right|^2}, \tag{22}$$

where $N_{gen} = 2000000$, is the number of the PHSP MC events at generator level in this analysis.

To estimate the statistical uncertainties of the fit fractions, we repeat the calculation of fit fractions by randomly varying the fitted parameters according to the error matrix. Then, for each amplitude , we fit the resulting distribution with a Gaussian function, whose width gives the corresponding statistical uncertainty.

5.5 Fit Result

The Dalitz plot of $m^2(K^+K^-)$ versus $m^2(K^-\pi^+)$ is shown in Fig.16. In the plot, we can see a clear peak of $K^*(892)^0$ and $\phi(1020)^0$. In the fit, the magnitude and phase of the amplitude $D_s^+ \to K^*(892)^0 K^+$ is fixed to 1.0 and 0.0, and the magnitudes and phases of the amplitudes are allowed to float.
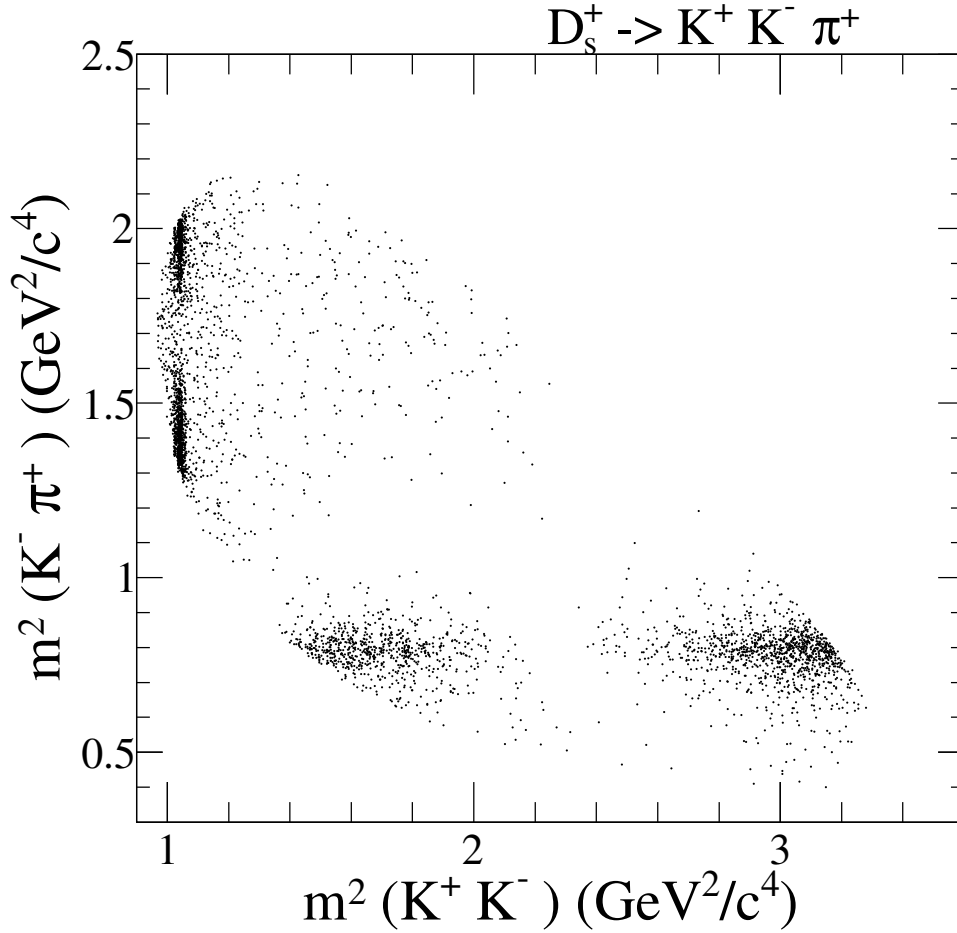
Figure 16: The plot of $m^2(K^+K^-)$ versus $m^2(K^-\pi^+)$ after event selection.

With the requiring the statistical significance larger than 5 standard deviations, there are 6 intermediate prcocess, $D_s^+ \to \bar{K}^*(892)^0 K^+$, $D_s^+ \to \phi(1020)\pi^+$, $D_s^+ \to f_0(980)\pi^+/a_0(980)\pi^+$, $D_s^+ \to \bar{K}_0^*(1430)^0 K^+$, $D_s^+ \to f_0(1370)\pi^+$, $D_s^+ \to f_0(1710)\pi^+$ are retained in final result. The statistical significance of the three amplitudes in final result are also checked.

With one amplitude dropped and the fit repeated, compared with the nominal fit the likelihood shift($\Delta \ln L$) and the number of freedom degree shift(Δn_{par}) are then corrresponding to the statistical significance. The detail $\Delta \ln L$, Δn_{par}, and the statistical significance for each amplitude are listed in Table 4. We also tested some other intermediate resonances. With each tested amplitude added and fit repeated, we get the corresponding likelihood shift($\Delta \ln L$), the number of freedom degree shift(Δn_{par}) and he statistical significance. And the results are listed in Table 5. As the statistical significances of the amplitudes listed in Table 5 are < 5, we did not retain them in the nominal fit.

The detail magnitudes, phases and fit fractions for the six amplitudes are listed in Table 6.

The Dalitz plot projections are shown in Fig.17.

Table 4: The $\Delta \ln L$, Δn_{par}, and the statistical significance for each amplitude

Amplitude	$\Delta \ln L$	Δn_{par}	Stat. significance
$D_s^+ \to \bar{K}^*(892)^0 K^+$	1959.3	2	>20
$D_s^+ \to \phi(1020)\pi^+$	2303.3	2	>20
$D_s^+ \to f_0(980)\pi^+/a_0(980)\pi^+$	270.5	2	>20
$D_s^+ \to \bar{K}_0^*(1430)^0 K^+$	39.4	2	8.6
$D_s^+ \to f_0(1710)\pi^+$	44.7	2	9.2
$D_s^+ \to f_0(1370)\pi^+$	22.5	2	6.4

Table 5: The $\Delta \ln L$, Δn_{par}, and the statistical significance for tested amplitudes

Amplitude	$\Delta \ln L$	Δn_{par}	Stat. significance
$D_s^+ \to f_0(1500)\pi^+$	0.8	2	0.8
$D_s^+ \to \phi(1680)\pi^+$	1.8	2	1.4
$D_s^+ \to f_2(1270)\pi^+$	4.5	2	2.5
$D_s^+ \to f_2(1525)\pi^+$	0.2	2	0.2
$D_s^+ \to \bar{K}_1^*(1410)^0 K^+$	4.8	2	2.6
$D_s^+ \to \bar{K}_1^*(1680)^0 K^+$	0.1	2	0.1
$D_s^+ \to \bar{K}_2^*(1430)^0 K^+$	2.8	2	1.9
non-resonance	6.4	2	3.1

Table 6: The magnitudes, phases and fit fractions for the six amplitudes

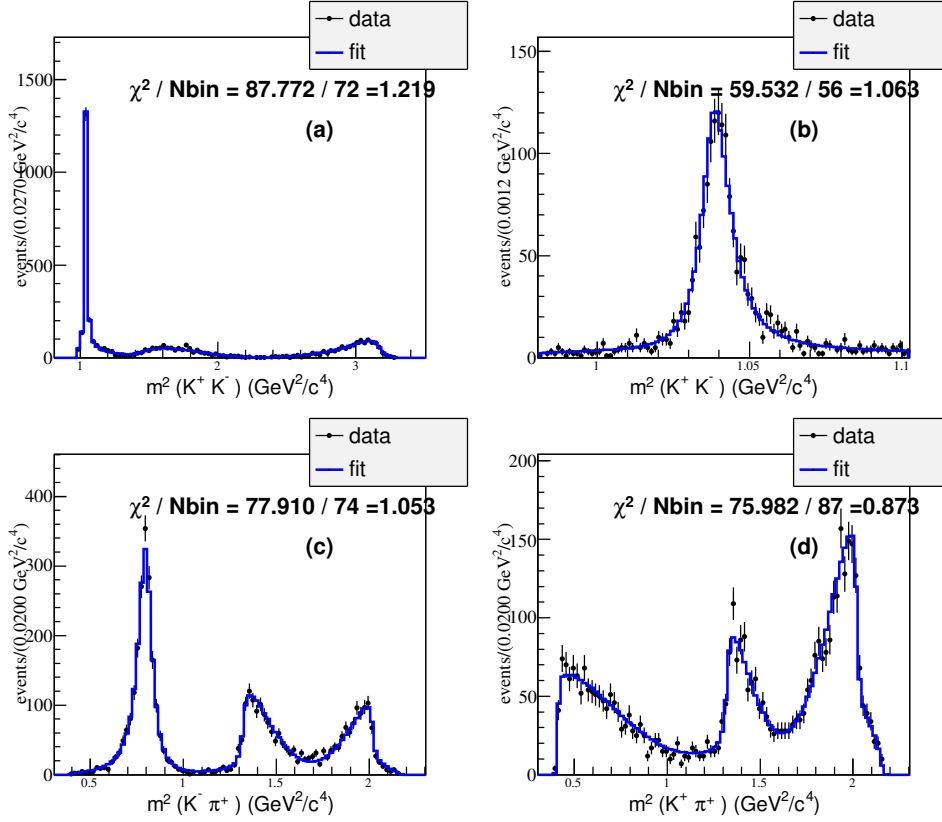| Amplitude	Magnitude	Phase	Fit fractions(%)
$D_s^+ \to \bar{K}^*(892)^0 K^+$	1.0(fixed)	0.0(fixed)	48.3±0.9
$D_s^+ \to \phi(1020)\pi^+$	1.09±0.02	6.22±0.07	40.5±0.7
$D_s^+ \to f_0(980)\pi^+/a_0(980)\pi^+$	2.88±0.14	4.77±0.07	19.3±1.7
$D_s^+ \to \bar{K}_0^*(1430)^0 K^+$	1.26±0.14	2.91±0.20	3.0±0.6
$D_s^+ \to f_0(1710)\pi^+$	0.79±0.08	1.02±0.12	1.9±0.4
$D_s^+ \to f_0(1370)\pi^+$	0.58±0.08	0.59±0.17	1.2±0.4

Figure 17: $D_s^+ \rightarrow K^+K^-\pi^+$: Dalitz plot projections from the nominal fit. The data are represented by points with error bars , the fit results by the histograms.

The goodness of the nominal fit is $\chi^2 = 290.1/280 = 1.04$.

5.6 Sytematic Uncertainties

Systematic uncertainties takein account:

- I Variation of resonance masses and widths within 1σ error.

    - For $f_0(980)/a_0(980)$, the mass and width are shifted within errors from Eq.12 in model inde-
      pendent PWA part.

    - For $f_0(1370)$, the mass and width are shifted within erros from [13].

    - For other states, errors used here are taken from PDG [12].

- II Variation of the effective radius of Blatt-Weisskopf Barrier within the range $[1.0, 5.0]\,GeV^{-1}$ for
  intermediate resonances and $[3.0, 7.0]\,GeV^{-1}$ for D_s meson.

- III Fit bias. The possible bias is given by the result from pull distribution check. With the results
  obtained from the fit, the signal MC samples are generated with the same size of the data. In this

Table 7: The results of pull distribution checks for the magnitudes, phases and fit fractions for the amplitudes

Amplitude	Phase		Magnitude		Fit fraction	
	mean	width	mean	width	mean	width
$D_s^+ \to \bar{K}^*(892)^0 K^+$					-0.13±0.04	0.98±0.03
$D_s^+ \to \phi(1020)\pi^+$	-0.04±0.05	1.00±0.03	0.07±0.04	0.95±0.03	0.01±0.04	0.95±0.03
$D_s^+ \to f_0(980)\pi^+/a_0(980)\pi^+$	-0.07±0.05	1.01±0.03	0.07±0.05	1.10±0.04	0.02±0.05	1.14±0.04
$D_s^+ \to \bar{K}_0^*(1430)^0 K^+$	0.00±0.05	1.11±0.04	0.14±0.04	0.95±0.03	0.10±0.04	0.99±0.03
$D_s^+ \to f_0(1710)\pi^+$	0.00±0.04	0.98±0.03	0.08±0.04	0.97±0.03	0.01±0.04	0.99±0.03
$D_s^+ \to f_0(1370)\pi^+$	-0.11±0.05	1.10±0.04	0.21±0.04	0.99±0.03	0.15±0.04	0.98±0.03

1   analysis, 300 MC samples with the size equaling to data are used to perform the pull distribution

2   check. The results are listed in Table7. The corresponding plots are shown in Fig.18, Fig.19 and
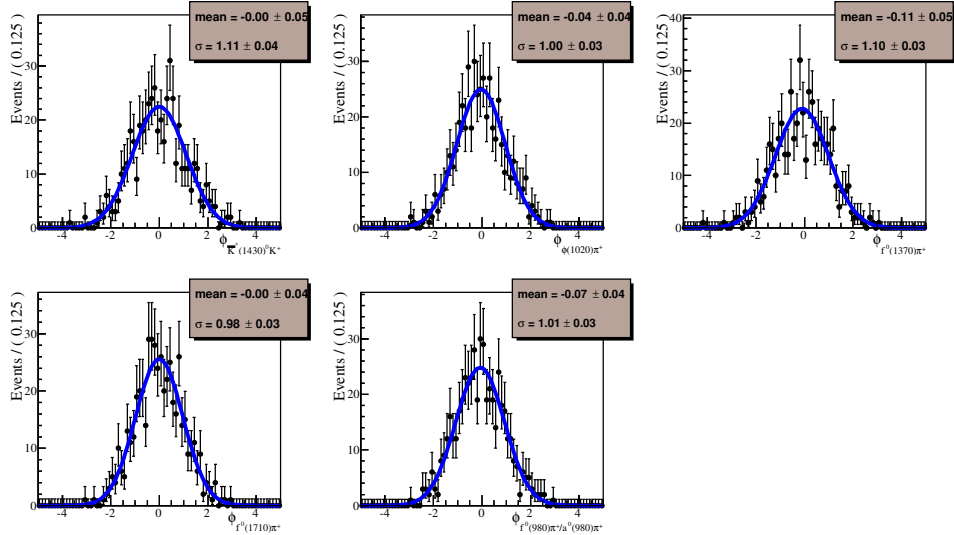
3   Fig.20.

Figure 18: The pull distribution check results for phases of the amplitudes in the nominal fit model.

4   Thus, the detail results of the systematic uncertainties are summarized in Table8. The final results of

5   the amplitude analysis are then listed in Tabl.13.

Table 8: Systematic uncertainties on the ϕ and FFs for different amplitudes in units of the corresponding statistical uncertainties.

Amplitude		Source			
		I	II	III	Total
$D_s^+ \to \bar{K}^*(892)^0 K^+$	FF	0.32	0.29	0.13	0.46
	ϕ	0.49	0.10	0.06	0.51
$D_s^+ \to \phi(1020)\pi^+$	ρ	0.49	0.14	0.18	0.54
	FF	0.44	1.13	0.05	1.21
	ϕ	0.98	0.25	0.06	1.01
$D_s^+ \to f_0(980)\pi^+/a_0(980)\pi^+$	ρ	1.11	0.17	0.10	1.13
	FF	1.16	0.15	0.06	1.17
	ϕ	1.02	0.48	0.09	1.13
$D_s^+ \to \bar{K}_0^*(1430)^0 K^+$	ρ	1.00	0.36	0.13	1.07
	FF	0.76	0.35	0.11	0.85
	ϕ	0.31	0.25	0.09	0.41
$D_s^+ \to f_0(1710)\pi^+$	ρ	1.17	1.23	0.07	1.70
	FF	0.71	1.21	0.05	1.41
	ϕ	2.66	0.27	0.11	2.67
$D_s^+ \to f_0(1370)\pi^+$	ρ	1.01	0.32	0.06	1.06
	FF	0.42	0.30	0.15	0.54

Table 9: The final results of the magnitudes, phases and fit fractions for the six amplitudes. The first and second uncertainties are the statistical and systematic uncertainties, respectively.

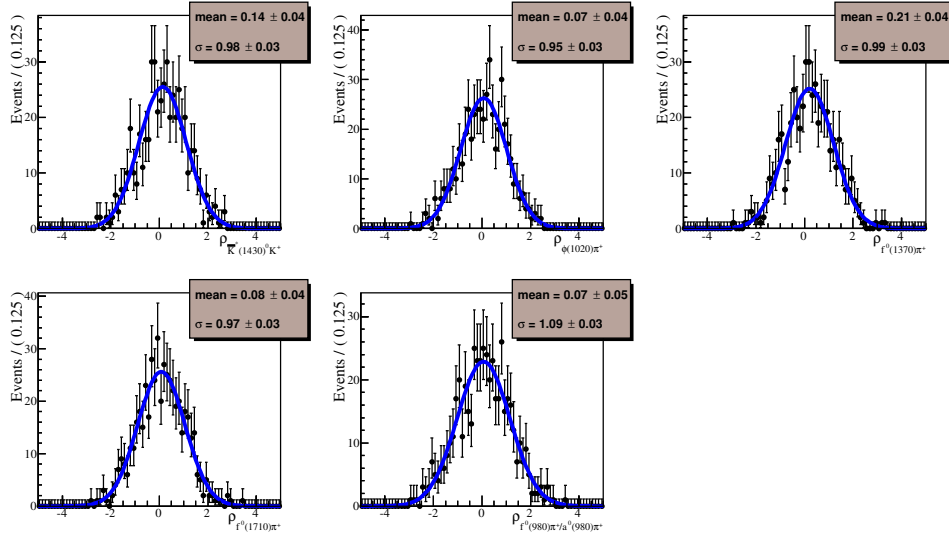| Amplitude	Magnitude	Phase	Fit fractions(%)
$D_s^+ \to \bar{K}^*(892)^0 K^+$	1.0(fixed)	0.0(fixed)	48.3±0.9±0.4
$D_s^+ \to \phi(1020)\pi^+$	1.09±0.02±0.01	6.22±0.07±0.04	40.5±0.7±0.9
$D_s^+ \to f_0(980)\pi^+/a_0(980)\pi^+$	2.88±0.14±0.16	4.77±0.07±0.07	19.3±1.7±2.0
$D_s^+ \to \bar{K}_0^*(1430)^0 K^+$	1.26±0.14±0.15	2.91±0.20±0.23	3.0±0.6±0.5
$D_s^+ \to f_0(1710)\pi^+$	0.79±0.08±0.14	1.02±0.12±0.05	1.9±0.4±0.6
$D_s^+ \to f_0(1370)\pi^+$	0.58±0.08±0.08	0.59±0.17±0.45	1.2±0.4±0.2

Figure 19: The pull distribution check results for magnitudes of the amplitudes in the nominal fit model.
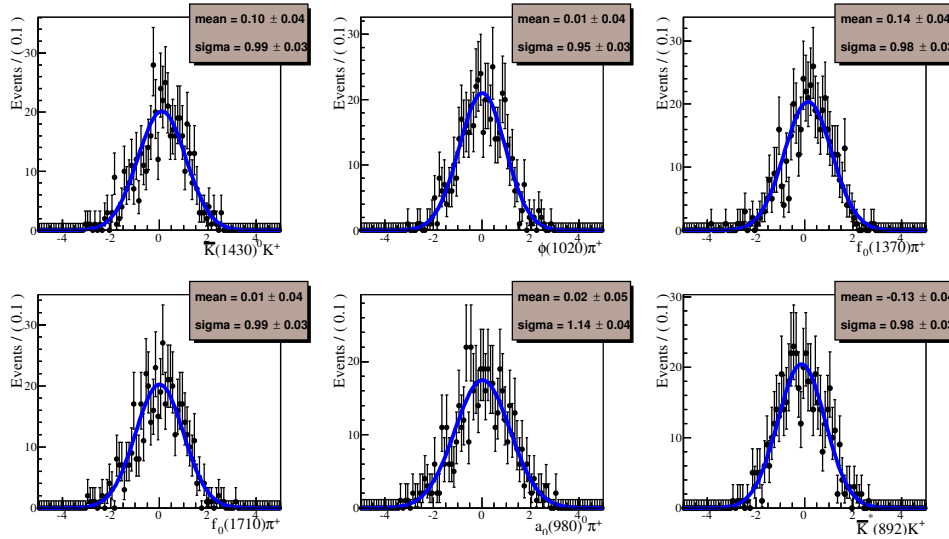

Figure 20: The pull distribution check results for fit fractions of the amplitudes in the nominal fit model.

Table 10: The ST yields(Y_{ST}) and ST efficiencies(ϵ_{ST}). The mass windows use the results in Ref. [9]

Tag mode	Mass window(GeV)	Y_{ST}	$\epsilon_{ST}(\%)$
$D_s^- \to K_S^0 K^-$	[1.948, 1.991]	965265 ± 1286	49.48 ± 0.07
$D_s^- \to K^+ K^- \pi^-$	[1.900, 2.030]	4254481 ± 2947	42.17 ± 0.03
$D_s^- \to K^+ K^- \pi^- \pi^0$	[1.947, 1.982]	1161036 ± 3400	10.61 ± 0.03
$D_s^- \to K_S^0 K^- \pi^+ \pi^-$	[1.958, 1.980]	233225 ± 1467	19.30 ± 0.12
$D_s^- \to K_S^0 K^+ \pi^- \pi^-$	[1.953, 1.983]	484801 ± 1312	22.72 ± 0.06
$D_s^- \to \pi^- \pi^- \pi^+$	[1.952, 1.984]	1152623 ± 3370	56.94 ± 0.17
$D_s^- \to \pi^- \eta'_{\pi^+ pi^- \eta_{\gamma\gamma}}$	[1.940, 1.996]	251617 ± 737	20.43 ± 0.06
$D_s^- \to K^- \pi^+ \pi^-$	[1.953, 1.983]	610925 ± 2902	47.18 ± 0.22

6 Branching Fraction Measurements

6.1 Event Selection for Branching Fraction Measurements

After the selection described in Set.3, we continue to select signals used in this part. We use the same 8 tag modes as in Sec.5.1. In the selection of tag D_s, for multiple candidates, the best candidate is chosen with M_{rec} closest to mass of D_s^* in PDF [12]. To further remove the background associated with the larger number of soft $\pi^\pm(\pi^0)$ from D_s^* decays, candidates are voted if the momentum of $\pi^\pm(\pi^0)$ is less than $0.1GeV$.

The single tag(ST) yields are extracted from the fits to the D_s invariant mass distributions, as shown in Fig.21. In the fit, the mass windows of the tag modes are set to be the same as the Ref. [9]. The signal shape is modeled as MC shape convoluted with a Gaussian function, whie background is parameterized as the 2nd-order Chebychev polynomial. The corresponding ST effeciencies are estimated from generic MC. The ST yields(Y_{ST}) and ST efficiencies(ϵ_{ST}) are listed in Table10

After selected the candidates of tag D_s, for each tag mode, we can get double tag candidates.

With the amplitude analysis results obtained from the fit to data, the double efficiencies without any kinematic fit requirement applied are determined and listed in Table11.

6.2 Analytic Strategy of Branching Fraction Measurement

The data sample for this analysis is collected at $E_{cm} = 4.178GeV$, about $100MeV$ higher than $D_s^* D_s$ threshold. Around this energy region, based on the cross section measurement by CLEO [6], we know that most D_s productionin $e^+ e^-$ collision comes from $D_s^{*\pm} D_s^\mp$ events with its cross section aprroximatedly $0.9nb$, while the cross section for $D_s^+ D_s^-$ is about a factor of 20 smaller. The D_s^* decays to either γD_s or $\pi^0 D_s$ with branching fractions of $(93.5 \pm 0.7)\%$ and $(5.8 \pm 0.7)\%$ [12], respectively. The other charm

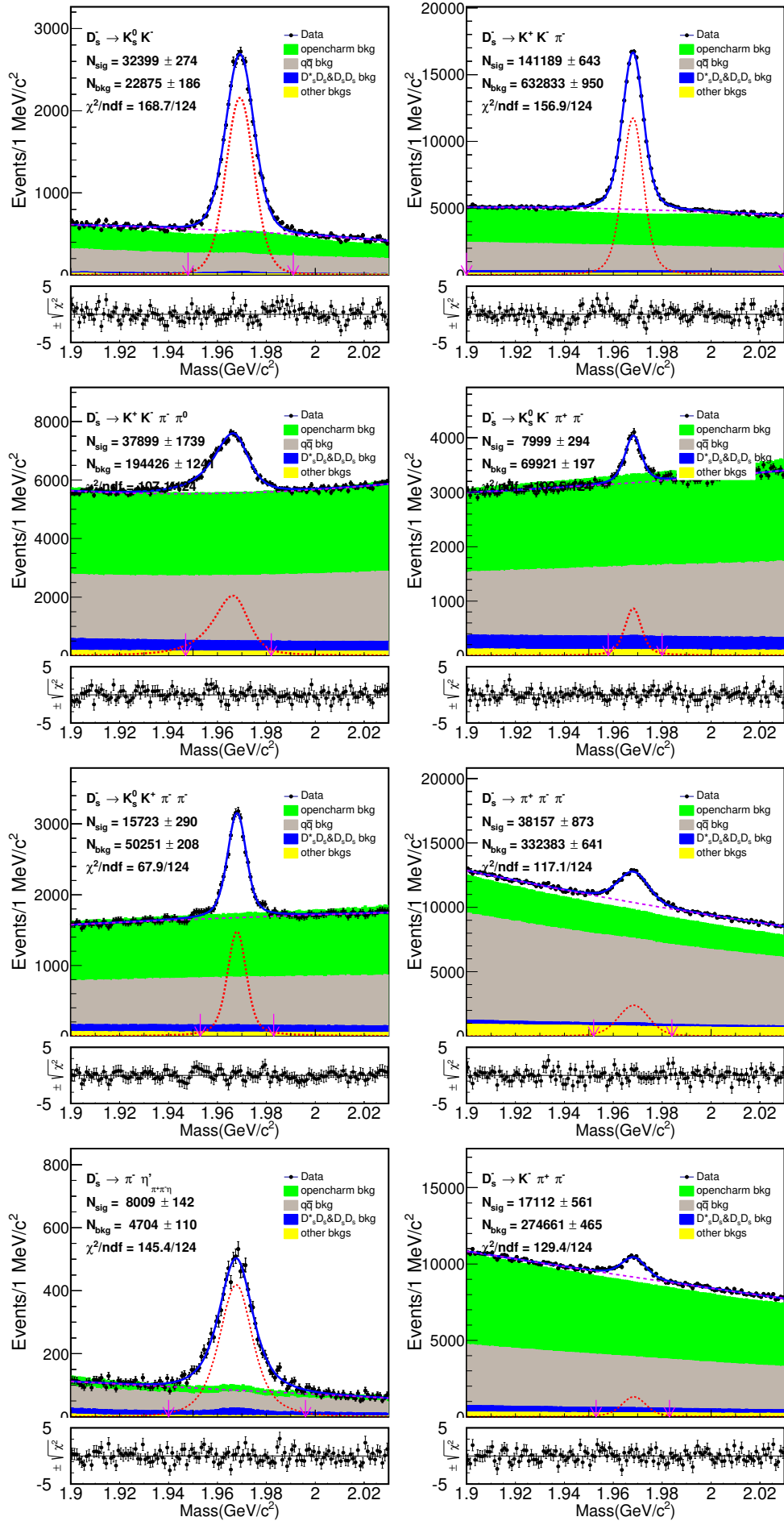Figure 21: Ds Mass fits from data. The points with error bars are data, and the blue line is the fit. Red short-dashed lines are signal, violet long-dashed lines are background. The red arrows denote the signal region.

Table 11: The DT efficiencies(ϵ_{DT}).

Tag mode	$\epsilon_{DT}(\%)$
$D_s^- \to K_S^0 K^-$	19.77±0.14
$D_s^- \to K^+ K^- \pi^-$	18.21±0.06
$D_s^- \to K^+ K^- \pi^- \pi^0$	4.69±0.03
$D_s^- \to K_S^0 K^- \pi^+ \pi^-$	8.34±0.11
$D_s^- \to K_S^0 K^+ \pi^- \pi^-$	9.55±0.09
$D_s^- \to \pi^- \pi^- \pi^+$	23.72±0.15
$D_s^- \to \pi^- \eta'_{\pi^+ pi^- \eta_{\gamma\gamma}}$	8.70±0.11
$D_s^- \to K^- \pi^+ \pi^-$	19.68±0.17

productions total $7pb$ mainly including $D^* \bar{D}^*$ with a cross section of $5nb$, $D^* \bar{D} + D \bar{D}^*$ with a cross section of $2nb$, and $D \bar{D}$ with a cross sectionof relatively small $0.2nb$. There also appears to be $D \bar{D}^* \pi$ production. The underlying light quark "continuum" background is about $12nb$. The relatively large cross sections, relatively large branching fractions, and sufficient luminosities allow us to employ double tag (DT) technique to study this study.

As $D_s^- \to K^+ K^- \pi^-$ is not only our signal mode but also one of our tag modes, we divide the events into two categories:

- Cat. A: Tag D_s decays to tag modes except $D_s^- \to K^+ K^- \pi^-$. The generic MC sample with the signal removed shows no peaking background around the fit range of $1.90 < M_{sig} < 2.03 GeV$. Thus, the double tag yield is determined by the fit to M_{sig}, which has shown in Fig.22(a).And the background is described with 2nd-order Chebychev polynomial. The double tag yield is 3503 ± 64.

- Cat. B: Tag D_s decays $K^+ K^- \pi^+$. As both of the two D_s mesons decay to our signal modes, we fit aM(the average mass of D_s at signal side and tag side), which is shown in Fig.22(b). Here, the background is described with 2nd-order Chebychev polynomial. The double tag yield is 1629 ± 43.

To measure the branching fraction of this decay, we start from the following equations with one tag mode:

$$N_{tag}^{obs} = 2N_{D_s^+ D_s^-} \mathcal{B}_{tag} \epsilon_{tag}, \tag{23}$$

$$\begin{aligned} N_{sig}^{obsA} &= 2N_{D_s^+ D_s^-} \mathcal{B}_{tag} \mathcal{B}_{sig} \epsilon_{tag,sig}, &\quad \text{for Cat. A} \\ N_{sig}^{obsB} &= N_{D_s^+ D_s^-} \mathcal{B}_{tag} \mathcal{B}_{sig} \epsilon_{tag,sig}, &\quad \text{for Cat. B} \end{aligned} \tag{24}$$

where $N_{D_s^+ D_s^-}$ is the total number of $D_s^{*\pm} D_s^{\mp}$ produced from $e^+ e^-$ collision; N_{tag}^{obs} is the number of observed tag modes; N_{sig}^{obsA} and N_{sig}^{obsB} are the number of observed signals for Cat. A and Cat. B, respectively;
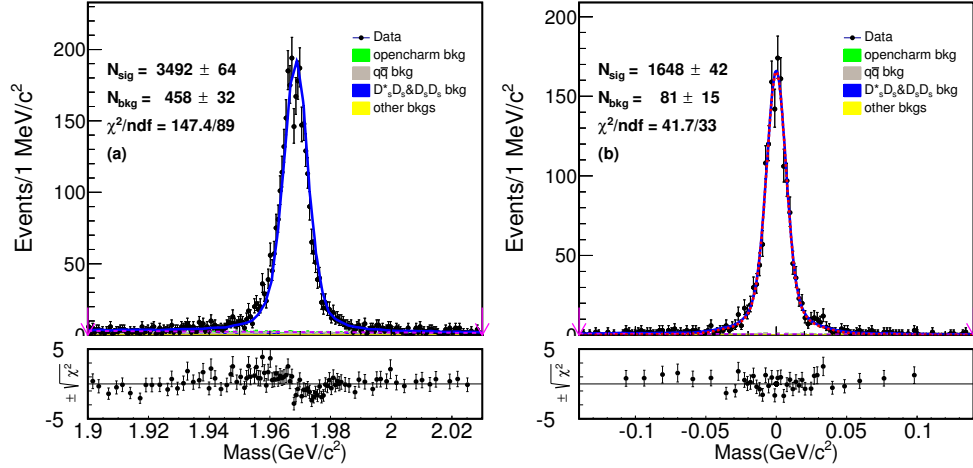
Figure 22: Fit of (a)Cat. A and (b)Cat. B. We fit M_{sig} and aM for Cat. A and Cat. B, respectively. The signal shapes are the corresponding simulated shapes convoluted with a Gaussian function and the background shapes are described with 2nd-order Chebychev polynomial.

$\mathcal{B}_{tag}$ and $\mathcal{B}_{sig}$ are the branching fractions of specific tag mode and signal mode, respectively; ϵ_{tag} is the reconstruction efficiency of the tag mode; $\epsilon_{tag,sig}$ is the reconstruction efficiency of both the tag and signal decay modes.

Using the above equations, it's easy to obtain:

$$\mathcal{B}_{sig} = \frac{N_{sig}^{obsA} + 2N_{sig}^{obsB}}{\sum_{\alpha} N_{tag}^{\alpha} \epsilon_{tag,sig}^{\alpha} / \epsilon_{tag}^{\alpha}}, \tag{25}$$

where the yields N_{tag}^{obsA}, N_{tag}^{obsB} and N_{tag}^{α} can be obtained from data, while ϵ_{tag} and $\epsilon_{tag,sig}$ can be obtained from the appropriate Monte-Carlo(MC) samples, $\alpha = 1, 2, 3...$ represents the tag mode.

6.3 Results of Branching Fraction

Then we can get the branching fraction $\mathcal{B}(D_s^+ \to K^+ K^- \pi^+) = (5.47 \pm 0.07)\%$(only statistical uncertainty) according to Eq.25.

6.4 Systematic Uncertainties

The following sources are taken in account to calculate systematic uncertainties.

- Signal shape. The systematic uncertainty due to the signal shape is studied with the fit without the Gaussian function convoluted, the double tag yield shift is taken as the related effect.

- Background shape and fit range. For background shape and the fit range, the MC shape is used to instead the 1st-order Chebychev polynomial and the fit range of $[1.90, 2.03]GeV$ is changed to $[1.89, 2.04]GeV$. The largest branching fraction shift is taken as the related effect.

Table 12: Systematic uncertainties of branching fraction.

Source	Sys. Uncertainty
Signal shale	0.3
Background shape and fit range	1.1
Fit bias	0.2
$K^{\pm}$ PID efficiency	1.1
$\pi^{\pm}$ PID efficiency	0.4
$K^{\pm}$ Tracking efficiency	1.1
$\pi^{\pm}$ Tracking efficiency	0.2
MC statistics	0.2
total	2.0

1 • Fit bias. The possible bias is estimated by the IO check with using the round 30-40 of generic MC.

2 • $K^{\pm}$ and $\pi^{\pm}$ Tracking/PID efficiency. Based on the works [16] and [17] by Xingyu Shan and

3 Sanqiang Qu, etc, we find that it's enough to assign 1.1% , 0.4%, 1.1% and 0.2% as the systematic

4 uncertainty for $K^{\pm}$ PID, $\pi^{\pm}$ PID, $K^{\pm}$ tracking, $\pi^{\pm}$ tracking efficiencies, respectively.

5 • MC statistics. The uncertainty of MC statistics is obtained by $\sqrt{\sum_i f_i \frac{\delta_{\epsilon_i}}{\epsilon_i} i}$, where f_i is the tag yield

6 fraction and ϵ_i is the signal efficiency of tag mode i.

7 All of the systematic uncertainties mentioned above are summarized in Table12.

8 The branching farction with systematic uncertainties is $\mathcal{B}(D_s^+ \rightarrow K^+K^-\pi^+) = (5.47 \pm 0.07_{stat.} \pm$

9 $0.11_{sys.})\%$.

Table 13: Comparision between BABAR, CLEO-c and this amplitude analysis.

Amplitude	BABAR	CLEO-c	This Analysis
$D_s^+ \to \bar{K}^*(892)^0 K^+$	47.9±0.5±0.5	47.4±1.5±0.4	48.3±0.9±0.4
$D_s^+ \to \phi(1020)\pi^+$	41.4±0.8±0.5	42.2±1.6±0.3	40.5±0.7±0.9
$D_s^+ \to f_0(980)\pi^+/a_0(980)\pi^+$	16.4±0.7±2.0	28.2±1.9±1.8	19.3±1.7±2.0
$D_s^+ \to \bar{K}_0^*(1430)^0 K^+$	2.4±0.3±1.0	3.9±0.5±0.5	3.0±0.6±0.5
$D_s^+ \to f_0(1710)\pi^+$	1.1±0.1±0.1	3.4±0.5±0.3	1.9±0.4±0.6
$D_s^+ \to f_0(1370)\pi^+$	1.1±0.1±0.2	4.3±0.6±0.5	1.2±0.4±0.2
$\sum FF(\%)$	110.2±0.6±2.0	129.5±4.4±2.0	114.2±1.7±2.3
χ^2/NDF	$\frac{2843}{2305-14} = 1.2$	$\frac{178}{117} = 1.5$	$\frac{290}{291-10-1} = 1.04$
Events	96307 ± 369(purity 95%)	14400(purity 85%)	4381(purity 99.7%)

Table 14: Comparisions of branching fractiong between BABAR, CLEO-c and this analysis.

$\mathcal{B}(D_s^+ \to K^+K^-\pi^+)(\%)$	TECN
$5.55 \pm 0.14_{stat.} \pm 0.13_{sys.}$	CLEO-c [18]
$5.06 \pm 0.15_{stat.} \pm 0.21_{sys.}$	BELLE [19]
$5.78 \pm 0.20_{stat.} \pm 0.30_{sys.}$	BABAR [20]
$5.47 \pm 0.07_{stat.} \pm 0.11_{sys.}$	This Analysis(BESIII)

7 Summary

This analysis presents the amplitude analysis for the decay $D_s^+ \to K^+K^-\pi^+$. Below is a comparison of amplitude analysis between BABAR, CLEO-c and this analysis. Our results are roughly consistent with those of BABAR and CLEO-c. And for the fit fraction of $D_s^+ \to f_0(980)\pi^+/a_0(980)\pi^+$, we tend to agree the result of BABAR.

In this analysis, as $a_0(980)$ and $f_0(980)$ are close to each other and parameters of $f_0(980)$ is not well measured, we have to take $f_0(980)$ and $a_0(980)$ as a whole, that is the $\mathcal{S}$ wave at the low end of K^+K^- mass spectrum. The $\mathcal{S}$ wave is extracted with the model independent method.

We also measured the branching farction and the value is $\mathcal{B}(D_s^+ \to K^+K^-\pi^+) = (5.47 \pm 0.07_{stat.} \pm 0.11_{sys.})\%$. As is shown in Table 14, the branching fraction of this analysis has the best precision.

References

[1] Yu Lu and Liaoyuan Dong, BESIII DocDB 682-v7.

[2] B. Aubert *et al.* (BABAR Collaboration), Phys. Rev. D**74**, 032003 (2006).

[3] M. Ablikim *et al.* (BES2 Collaboration), Phys. Rev. D**72**, 092002 (2005).

[4] V.V. Anisovich *et al.*, PAN **65** 1545 (2002).

[5] D.Cronin-Hennessy *et al.* (CLEO Collaboration), Phys. Rev. D**80**, 072001 (2009).

[6] P.del Amo Sanchez *et al.* (BARBAR Collaboration), Phys. Rev. D**83**, 052001 (2011).

[7] Andy Julin, Hajime Muramatsu and Ron Poling, BESIII DocDB 580-v1.

[8] C. Patrignani *et al.* (Paritcle Data Group), Chin. Phys. C 40,100001 (2016)

[9] Sifan Zhang and Hailong Ma, BESIII DocDB 630-v35.

[10] Yu Lu and Liaoyuan Dong, BESIII DocDB 416-v30.

[11] B. S. Zou and D. V. Bugg, Eur. Phys. J. A**16**, 537(2003).

[12] K. A. Olive *et al.* (Particle Data Group), Chin. Phys. C **40**, 100001 (2016)

[13] M. Alblikim *et al.* (BESIII Collaboration), Phys. Lett. B**607** 243 (2005).

[14] G. Bonvicini *et al.* (CLEO Collaboration), Phys. Rev. D**78**, 052001 (2001).

[15] Yu Lu and Liaoyuan Dong, BESIII DocDB 613-v16.

[16] https://indico.ihep.ac.cn/event/8006/contribution/1/material/slides/0.pdf

[17] https://indico.ihep.ac.cn/event/8023/contribution/1/material/slides/0.pdf

[18] P.U.E. Onyisi *et al.* (CLEO Collaboration), Phys. Rev. D**88**, 032009 (2013).

[19] A. Zupanc *et al.* (BELLE Collaboration), JHEP **1309**, 139 (2013).

[20] P. del Amo Sanchez *et al.* (BABAR Collaboration), Phys. Rev. D**82**, 091003 (2010).

Appendices

A To be supplemented